Chapter 5

Structural and Mechanical Behaviour of Al-Fe Intermetallics

Mohammed Ishaq Raviathul Basariya and
Nilay Krishna Mukhopadhyay

Additional information is available at the end of the chapter

http://dx.doi.org/10.5772/intechopen.73944

Abstract

In this chapter, results of our recent investigations on Al-25%Fe (at.%), Al-30%Fe and Al-34.5%Fe alloys close to Al_3Fe, Al_5Fe_2 and Al_2Fe intermetallic phases have been discussed. The effect of process parameters on structural aspects and mechanical behaviour of Al-Fe intermetallics has been studied. The high melting intermetallics that are difficult to prepare by conventional processing technique are easily synthesized in nanocrystalline state with a homogeneous structure by mechanical means. In this process, we have come out with a single orthorhombic Al_5Fe_2 nanocrystalline intermetallic phase. Hardness measurements of intermetallic revealed an increase in hardness with a decreasing grain size up to a critical grain size, followed by a decrease. A decrease in hardness with a grain size refinement, an indication of softening behaviour, demonstrating the Inverse Hall-Petch (IHP)-like phenomenon has been observed in intermetallic compounds. The deviation from the regular Hall-Petch (HP) behaviour has been discussed using various deformation models based on the dislocations and grain boundary-mediated processes. The study is focused on investigations of Al-rich iron aluminide intermetallics to understand the structure property correlations.

Keywords: high-energy ball milling, intermetallics, Al_5Fe_2, Al_3Fe, inverse Hall-Petch, nanostructured materials, mechanical properties, deformation mechanisms, grain boundary sliding

1. Introduction

Intermetallics represent a manifold class of materials that possess intermediate properties between metallic and non-metallic materials. Intermetallic phases and compounds are formed by a combination of two or more metals falling at or near a fixed stoichiometric ratio

and exhibit different crystal structure and properties than their constituent elements. The composition of an intermetallic may vary within a restricted composition range known as homogeneity range. Since 2500 BC, metallurgists have used intermetallics, and its phases have attracted significant interests during the last few decades since they offer new prospects for developing structural materials for high-temperature applications.

1.1. Intermetallics

An increased need for new and novel materials with specified properties and particular application has attracted greater attention of metallurgists and material scientists in recent years. Intermetallics are one such material with a vast potential for application in a wide range of technologically important areas [1]. The first observation of an intermetallic was made in 1839 by Karl Karsten, when he observed a discontinuity in the action of acids on alloys of copper and zinc at the equi-atomic composition and suggested the formation of a compound. The compound is now popularly called as β-brass (CuZn). Intermetallics are already indispensable in many applications and offer the possibility of providing additional breakthrough in performance in, for example, high-temperature structural materials, magnetic materials and hydrogen storage materials. As a by-product of amorphization studies or alloying development, nanocrystalline intermetallic compounds can be synthesized. Nanocrystalline intermetallics possess improved mechanical properties at an ambient temperature. Bohn et al. [2] have suggested that nanocrystalline intermetallic compounds may have improved mechanical properties. Their study concludes several possible ways of improving strength and ductility. However, the strength of elemental nanocrystalline metals can be increased by factors of 4–5 over conventional grain size materials [3], strengthening effects in some hard intermetallics that are more modest of the order of 10–20% [4]. The brittle nature of most intermetallics requires powder metallurgical processing route. Amorphization of intermetallic compounds by mechanical alloying (MA) was first reported by Ermakov et al. [5, 6] in Y-Co and Gd-Co systems. Amorphous phases from elemental powder mixtures or powders of intermetallics synthesized by high-energy ball milling have attained an unprecedented interest. A polymorphous phase transformation from crystalline phase to amorphous phase can occur when the free energy of an intermetallic compound is raised by severe mechanical deformation above that of the amorphous phase. The observed transformation could be ascribed to an increased volume fraction of grain boundaries and simultaneous disordering [7]. Zou et al. [8] reported the formation of amorphous phase in Al-Fe alloy at early stages of MA. It has also been reported that during prolonged milling, amorphous phase undergoes crystallization to form intermetallics.

1.2. Al-Fe intermetallics

Considering all excellent physical and mechanical properties of aluminium, it has become an important element in intermetallics. Iron (Fe) and aluminium (Al) alloys rank among the most important engineering materials because they provide good properties at a low material cost in many applications [9]. Iron aluminide compounds are solid examples of the use of aluminium in intermetallics industry. Changing the aluminium content in iron-aluminium system leads to different iron aluminide compounds. Al-rich iron aluminides are characterized by low density, but also by lower strength and hardness than Fe_3Al or FeAl ones. However, the strength and

Phases	Symbol	Crystal structure	Stability range (at.%)	Vickers hardness (9.8 N)
AlFe	β″	BCC (Order)	23–55	491–667
$AlFe_3$	β′	DO_3	23–34	344–368
Al_2Fe	ζ	Triclinic	66–67	1058–1070
Al_5Fe_2	η	Orthorhombic	70–73	1000–1158
Al_3Fe	θ	Monoclinic	74.5–76.5	772–1017

Table 1. Crystal structure, stability range and hardness of intermetallic phases formed in Al-Fe binary systems at room temperature [10].

hardness can be improved by grain size refinement, especially to nanometric scale. Having their strength increased, Al-based intermetallics possess a high specific strength. **Table 1** indicates the crystal structure, stability range and hardness for the Al-Fe intermetallic phases. Studies on Al-Fe system have been concentrated mainly on mechanical alloying (MA) with individual elements [11–14]. Moreover, similar structures have been evidenced for a range of Al content. In Al-Fe intermetallic, Al_2Fe compound retains the lowest possible symmetry crystal structure, triclinic (Pearson symbol aP19) [15]. Due to its lowest symmetry, the triclinic phase transforms to a high-symmetry Al_5Fe_2 orthorhombic (Pearson symbol oC24) in the nearby composition. Stability calculations utilizing first principles total energy envisage that oC24 structure has a much lower atomic density than aP19 structure, resulting in a high vibrational entropy and hence aP19 structure loses stability to the oC24 structure at elevated temperatures [16].

1.3. Al-Fe intermetallics by mechanical alloying/mechanical milling

Nanocrystalline intermetallic compounds are said to have enhanced properties as compared to conventional grain-sized materials. MA/mechanical milling (MM) has been considered a suitable processing method capable of attaining this goal of producing nanostructured materials [9]. The synthesis of intermetallics through MA/MM has emerged as a valuable method for the following reasons: (1) the synthesis of intermetallics which are difficult to prepare by conventional methods, (2) to obtain enhanced properties through microstructural modifications and (3) the synthesis of nonequilibrium microstructures, such as amorphous alloys at intermetallic compositions. The formation of amorphous phase in Al-20 at.%Fe alloy was reported by Zhou et al. after 240 h of MA [17]. Almost complete amorphous phase in Al-(17–33) at.%Fe system was observed by Huang et al. [18]. In a similar study, for Al-34 at.%Fe, Al-25 at.%Fe, Al-25 at.%Fe and Al-20 at.%Fe system, respectively, crystalline phases were evidenced by Enzo et al. and Cardellini et al. [19, 20]. For a composition range of Al-34.7–35.3 at.%Fe intermetallic phase, Al_5Fe_2 along with Al_2Fe was observed by Gasior et al. [21]. A comparison of the phases formed in Al-Fe alloys as analysed from the X-ray diffraction (XRD) traces is given in **Table 2**. In addition to MA experiments, Romero et al. [22] reported the effect of mechanical milling (MM) on the structural evolution of as-cast Al_2Fe and Al_5Fe_2 intermetallic systems at different short milling times. Apart from this study, no other reports on systematic investigation on the structural evolution of as-cast Al-rich iron aluminide intermetallics are available. The possibility of nanostructured and amorphous phases and their stability by MM can

Alloy	Phases formed	References
Al-34.7–35.3 at.%Fe	Al_5Fe_2 + Al_2Fe	Gasior et al. [21]
Al-28.45 at.%Fe	Al_5Fe_2 + Al_2Fe	Romero et al. [22]
Al-25 at.%Fe	Al_5Fe_2	Cardellini et al. [20]
Al-20 at.%Fe	Amorphous	Zhou et al. [17]
Al-20 at.%Fe	Al_5Fe_2	Cardellini et al. [20]
Al-34 at.%Fe	α-Al	Enzo et al. [19]
Al-17–33 at.%Fe	Amorphous	Huang et al. [18]
Al-25 at.%Fe	α-Al	Enzo et al. [19]
Al-33.28 at.%Fe	Al_5Fe_2 + Al_2Fe	Romero et al. [22]

Table 2. List of phases formed in Al-Fe alloy.

be explored from the thermodynamic explanation based on a semi-experimental theory of improved Miedema's model (Zhang model) [23] by calculating the Gibbs free energy of the phases from their enthalpy of formation.

1.4. Nanostructured materials

Nanostructured materials are an important class of metastable materials that are produced by ball milling. Materials are considered as nanostructured if the crystallite size is of the order of few nanometres (typically 1–100 nm). A novel way of transforming a material to a metastable state is to reduce its grain size from micrometres to nanometres, when the proportion of atoms at the grain boundaries is equal to or higher than those inside the grains. The fine grain-sized materials are structurally characterized by a large volume fraction of atoms in or near the grain boundaries, which significantly alter the material properties that are often superior or sometimes completely new in comparison with conventional coarse-grained polycrystalline materials. In 1987, Thompson and Politis first reported the formation of a nanostructured material synthesized by MA [24]. A mechanism for the formation of nanostructures by MA/MM has been reported [25]. In 1992, Li et al. proposed a relation between grain size and the time of milling by a model for the refinement of grain size during ball milling [26].

It is given by

$$d = K t^{-2/3} \tag{1}$$

where d is the grain size, t is the time and K is a constant.

The balance between defect/dislocation structure introduced by the plastic deformation of milling and its recovery processes forms the main criteria to decide on the minimum grain size that can be achieved by mechanical milling. This process will result in a lower bound for the grain size of pure metals and alloys and reveals that a small grain size itself provides a limit for further grain refinement on milling. On the whole, when the material exhibits a nanocrystalline

structure, hence microstructural refinement cannot be observed and further deformation can only be accomplished by grain boundary sliding (GBS). It has been suggested that the minimum grain size that can be achieved by milling is determined by the balance between defect/dislocation structure introduced by the plastic deformation of milling and its recovery by thermal processes. This contributes to a lower bound for the grain size of pure metals and alloys and reveals that a small grain size itself provides a limit for further grain refinement on milling. Once the whole material exhibits a nanocrystalline structure, further deformation can only be accomplished by grain boundary sliding, and hence microstructural refinement cannot be observed. The limiting grain size is normally determined by the minimum grain size that can sustain a dislocation pile-up within a grain and by the rate of recovery [27]. Earlier researchers have proposed that hardness decreases at small grain sizes as it becomes impossible to accommodate the high density of dislocations required to form a pile-up at a grain boundary [28, 29].

2. Effect of process parameters on mechanical properties

Despite the same composition of initial powder mixture, various structures can evolve depending on the parameters of the milling process. In this section, the effect of mechanical milling (MM) on the structural evolution of as-cast Al-rich iron aluminide intermetallics through different stages of milling and its mechanical behaviour has been discussed. The mechanical properties of intermetallics are closely related to their structure and its stability [30]. Grain boundaries are the most important microstructural elements of materials, and their strengthening effect is phenomenologically quantified by a classical HP relationship. However, deviations from HP relation contributing to a softening behaviour are also observed after a critical grain size (d_c). Due to the difference in the mechanical properties, which is greatly influenced by the microstructure [31, 32] of the intermetallic phases and its transformation during milling, a significant difference in the force displacement curves manifested not only by the shapes of the load-penetration depth but also by the maximum penetration depth attained under the same conditions was observed when evaluated using Oliver and Pharr method [33] (Oliver et al. (2004)). For intermetallics that are concerned, the effort has been directed mainly towards the development of high strength materials, and reports that address softening behaviour in nanoscale microstructures or composite microstructures are very rare. Al-25 at.%Fe, Al-30 at.%Fe and Al-34.5 at.% Fe close to Al_3Fe, Al_5Fe_2 and Al_2Fe intermetallic phases have been prepared in an arc-melting furnace under argon atmosphere. The pre-alloyed ingots were brittle and therefore repeatedly crushed and mechanically sieved to powders. Mechanical milling of the crushed powders was then carried out using high-energy planetary ball mill. This study provides some insights to understand the correlation between the process parameters and the mechanical behaviour of Al-Fe intermetallics.

2.1. Microstructural and structural features

Figure 1 shows X-ray diffraction pattern of crushed as-cast powders of Al-25 at.%Fe alloy. Diffraction peaks confirm mostly single-phase complex monoclinic Al_3Fe (θ) structure. **Figure 2** shows the structural evolution of Al_3Fe intermetallic subjected to varying hours of MM. A relatively broad peak was observed because of the fine crystallite size and the presence of strain in

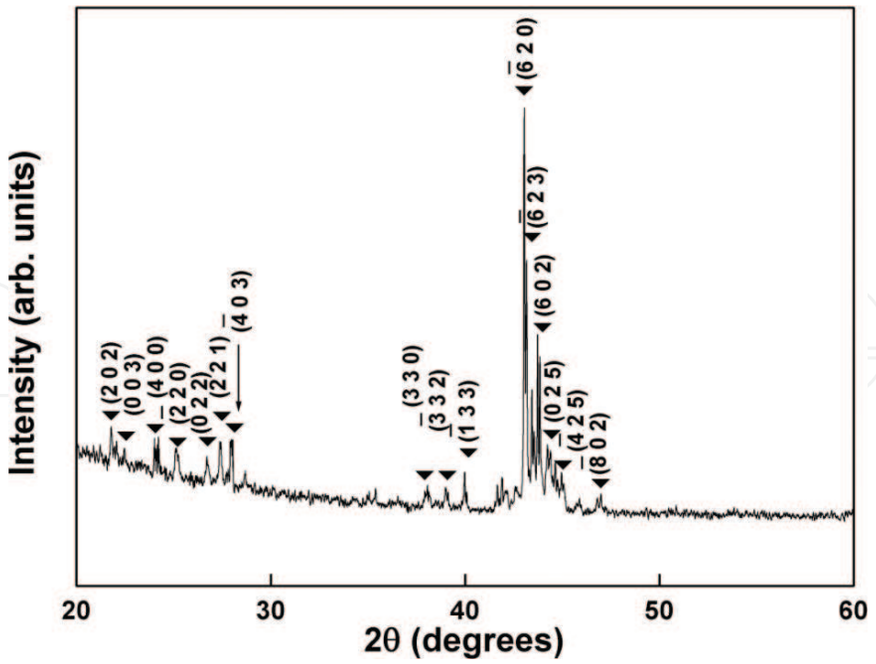

Figure 1. XRD pattern of Al-25 at.%Fe as-cast alloy showing single θ-Al_3Fe intermetallic phase (reprinted with kind permission from reference [34], copyright 2015, Elsevier).

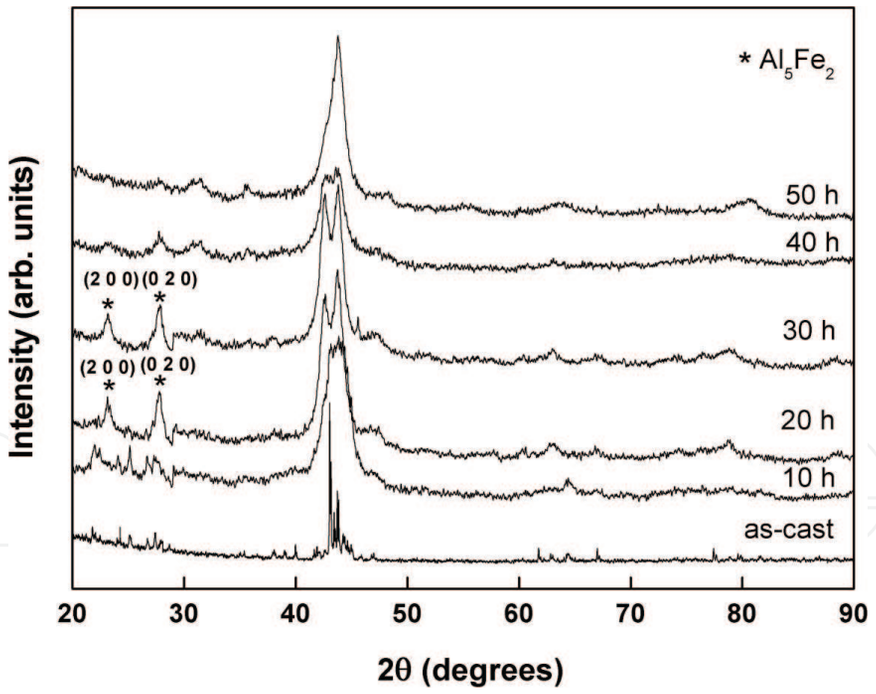

Figure 2. XRD patterns showing structural evolution of θ-Al_3Fe intermetallic phase (reprinted with kind permission from reference [34], copyright 2015, Elsevier).

the powder at early stages of milling. After 10–20 h of milling, the formation of η-Al_5Fe_2 was evidenced as an intermediate phase. The presence of η-Al_5Fe_2 prevailed till 30 h of milling, but a further increase in the milling time led to the broadening of these peaks too. The intermetallic Al_3Fe phase was completely transformed into the amorphous state after 50 h of milling. A broad

http://dx.doi.org/10.5772/intechopen.73944

halo at 2θ = 40–47° suggests that the formation of an amorphous phase was seen from the XRD patterns shown in **Figure 2**. Eventually, the phase transformations during MM for Al–25 at.%Fe alloy powders are expressed as follows:

$$\theta - Al_3Fe \rightarrow (\theta - Al_3Fe + \eta - Al_5Fe_2) \rightarrow (\eta - Al_5Fe_2 + \text{Amorphous}) \rightarrow \text{Amorphous}. \quad (2)$$

Transmission electron microscope (TEM) image of Al-25 at.%Fe alloy milled for 50 h is shown in **Figure 3**. The micrograph showed the co-existence of nanocrystalline, η-Al_5Fe_2 and amorphous phases, and a diffuse ring along with diffraction spots was evidenced in a selected area diffraction (SAD) pattern. However, complete amorphization after 50 h of milling was observed in its corresponding XRD pattern. The broadening of the peak observed in XRD corresponds not only to the formation of amorphous structure but also to the refinement of the nanocrystalline structure induced by mechanical milling, and hence residual crystalline phase is present along with amorphous phase. The characteristic X-ray diffraction pattern of as-cast powders of Al-30 at.% Fe alloy is shown in **Figure 4**. The most intense diffraction peaks (2 2 1) and (3 1 1) at 2θ = 42.55 and 43.79 were found in the as-cast alloy. JCPDS data suggest that this compound is representative of a single Al_5Fe_2 orthorhombic phase (JCPDS reference code: 00-047-1435) [36] with lattice parameters of a = 0.7648 nm, b = 0.6413 nm and c = 0.4216 nm. Results of XRD patterns showing the structural evolution of Al_5Fe_2 intermetallic subjected to MM for different ranges of milling time are shown in **Figure 5**. It is apparent that milling up to 30-h disappearance of all peaks except for major peaks of (2 2 1) and (3 1 1) was observed. The broadening observed in the diffraction peak can be attributed to the major peaks overlapping from the intermetallic phase. The results obtained are in contrary to Al_5Fe_2 obtained by MA route [11], where complete formation of intermetallic phase was achieved in Al-25%Fe

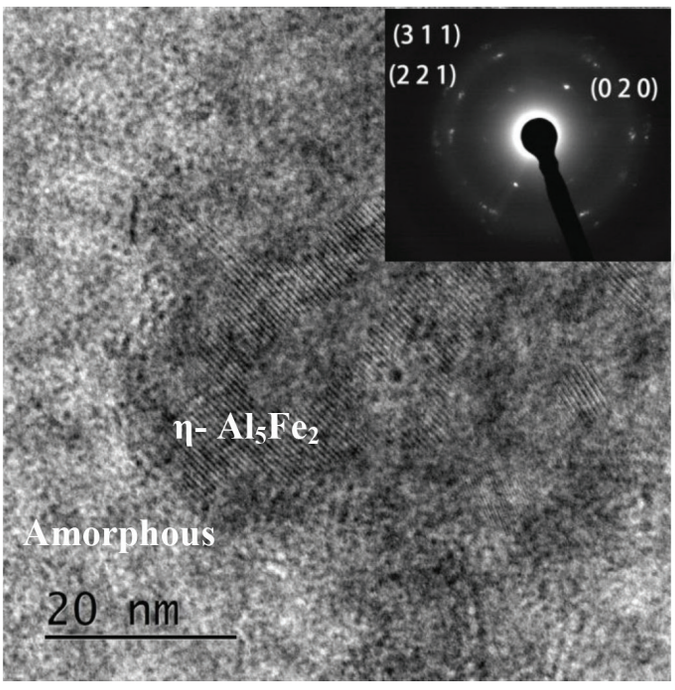

Figure 3. TEM image of 50 h milled product of Al-25 at.%Fe alloy showing crystalline η- Al_5Fe_2 and amorphous phase and its corresponding SAD pattern (reprinted with kind permission from reference [34], copyright 2015, Elsevier).

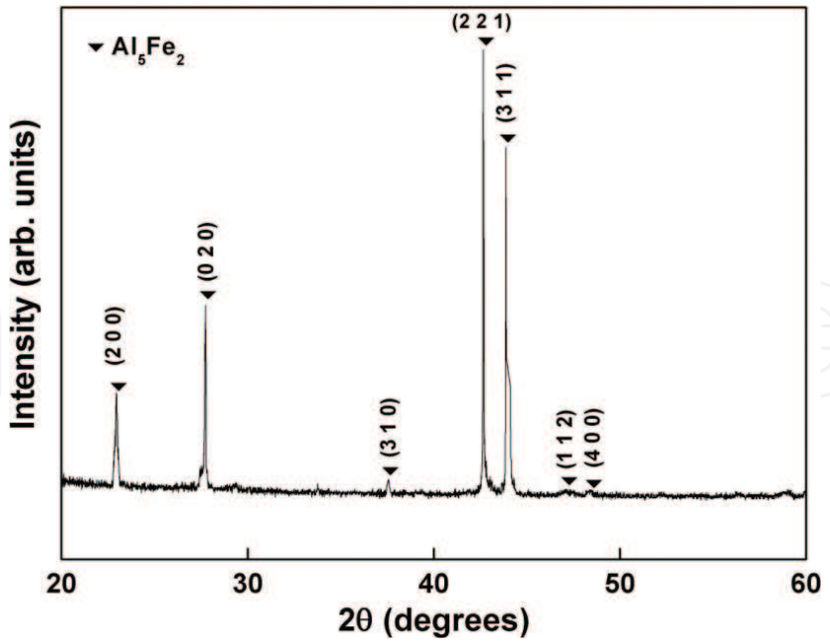

Figure 4. XRD pattern of as-cast Al-30 at.% Fe alloy (reprinted with kind permission from reference [35], copyright 2016, Taylor & Francis).

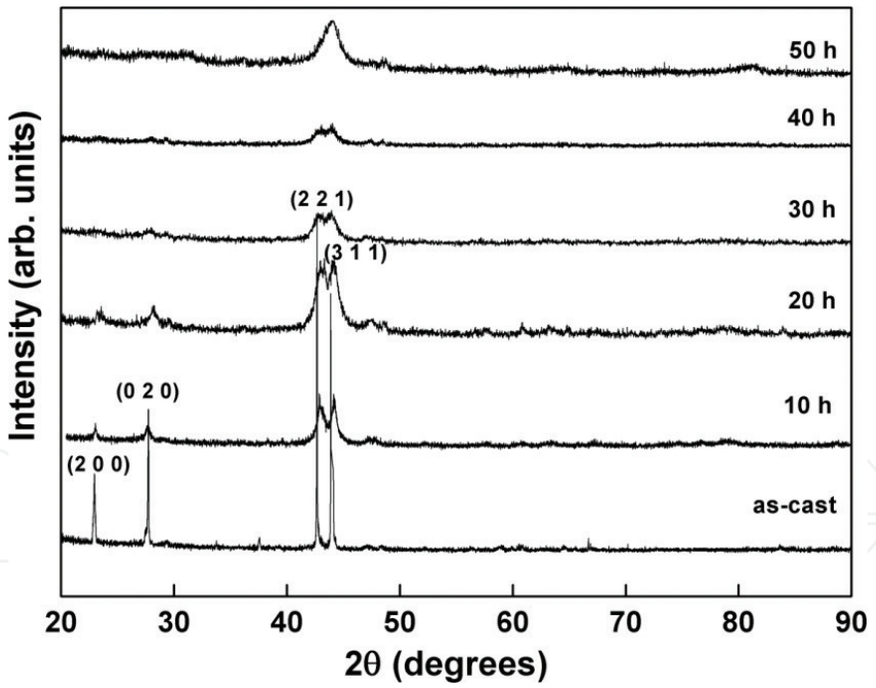

Figure 5. XRD patterns showing structural evolution of Al_5Fe_2 intermetallic during MM (reprinted with kind permission from reference [35], copyright 2016, Taylor & Francis).

after 30 h of MA, and the formation of amorphous phase was seen after 50 h of MA. Further in a similar work, Hunag et al. [18] observed the formation of the Al_5Fe_2 intermetallic in Al-24.4%Fe powder heat-treated at 500°C after MA for 180 h. It is interesting to note that the XRD peaks undergo broadening in the course of mechanical milling up to 50 h mainly due to cumulative effects of grain refinement and lattice strain. A bright field and dark-filed

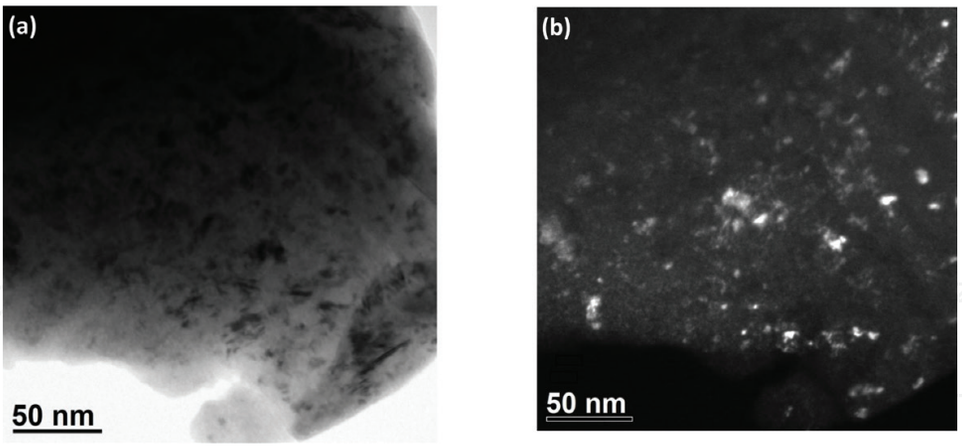

Figure 6. (a) Bright field image and (b) dark field image of 50 h milled powder of Al-30 at.% Fe alloy (reprinted with kind permission from reference [35], copyright 2016, Taylor & Francis).

image of 50 h-milled Al-30 at.% Fe alloy (**Figure 6a** and **b**) reveals the presence of a nano-crystalline structure suggesting the presence of a nanostructured Al_5Fe_2 intermetallic phase which agrees well with the structural evolution observed from the XRD pattern.

Figure 7 shows the XRD pattern of as-cast Al-34.5 at.%Fe alloy. Diffraction peak confirms a mixture of intermetallic phases namely ζ-Al_2Fe and η-Al_5Fe_2. For a compositional range of 34.7–35.3 at.%Fe in Al alloy, the observed intermetallic phase Al_5Fe_2 along with Al_2Fe was observed by Gasior et al. [21]. Phase transformation from crystalline triclinic Al_2Fe and orthorhombic Al_5Fe_2 to the partial formation of amorphous phase at 10 h of MM resulted in Al-34.5 at.%Fe alloy. Due to the peak overlapping from the mixture of intermetallic phases, a width was observed in the most, intense diffraction peak. With continued milling, a decrease

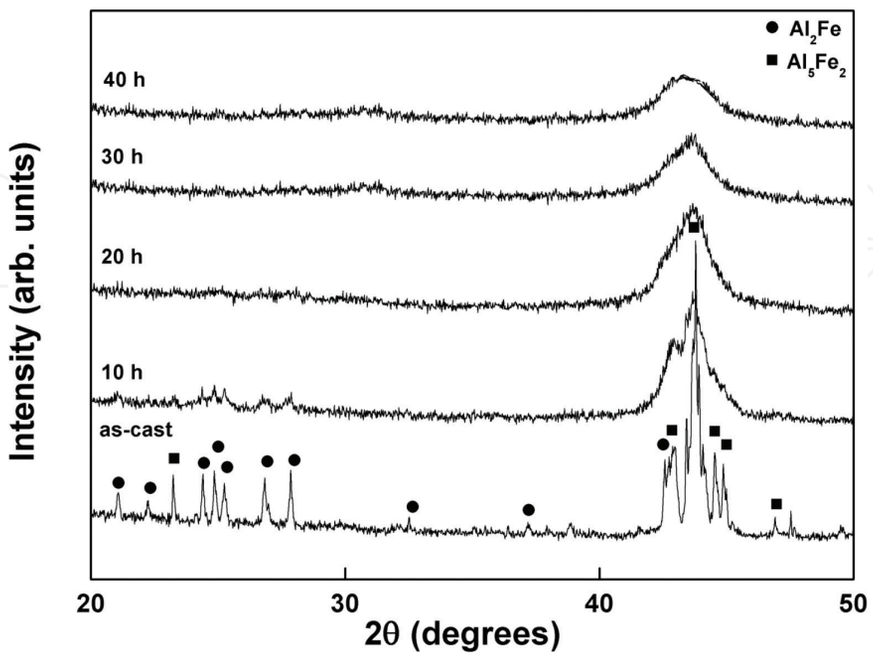

Figure 7. XRD patterns Al-35.4 at.%Fe as-cast alloy and after mechanically milled for various intervals showing structural evolution with milling time (reprinted with kind permission from reference [34], copyright 2015, Elsevier).

in the width of Bragg peaks and an increase in peak resolution were noted, indicating that Al_2Fe intermetallic phase becomes unstable as a result of MM. The detected phase transition that occurred during milling process is suggestive of the accumulation of structural defects which increases the stored energy in the intermetallic material.

As evidenced in **Figure 7**, complete amorphization after 40 h of milling was achieved in this particular composition with prolonged milling time. The fine grain size and consequently large surface area induced by MM make the powders of this particular composition pyrophoric in nature after 40 h of milling. The same was observed even when milling experiments were paused periodically at regular intervals of every 30 min. Phase transformations achieved as a result of MM for Al-34.5 at.%Fe alloy powders are expressed as.

$$\left(\zeta - Al_2Fe + \eta - Al_5Fe_2\right) \rightarrow \eta - Al_5Fe_2 \rightarrow \text{Amorphous.} \tag{3}$$

The orthorhombic structure of Al_5Fe_2 phase features a rigid framework of fully occupied Al and Fe sites as well as partially occupied Al sites confined within channels [37]. This kind of structure makes it unstable when subjected to a severe plastic deformation leading to an amorphous phase. Further, for the present milling conditions, Al_5Fe_2 phase was also found to be stable with respect to its competing phases. Due to lattice defects introduced by MM which promote spontaneous transformation to the amorphous phase, the intermetallic compounds with narrow homogeneity ranges tend to become amorphous [38]. A high-resolution TEM micrograph corresponding to Al-34.5 at.%Fe alloy milled for 40 h is shown in **Figure 8**. The micrograph reveals a single amorphous phase and is corroborated by the fast Fourier transformation-selected area diffraction (FFT-SAD) pattern.

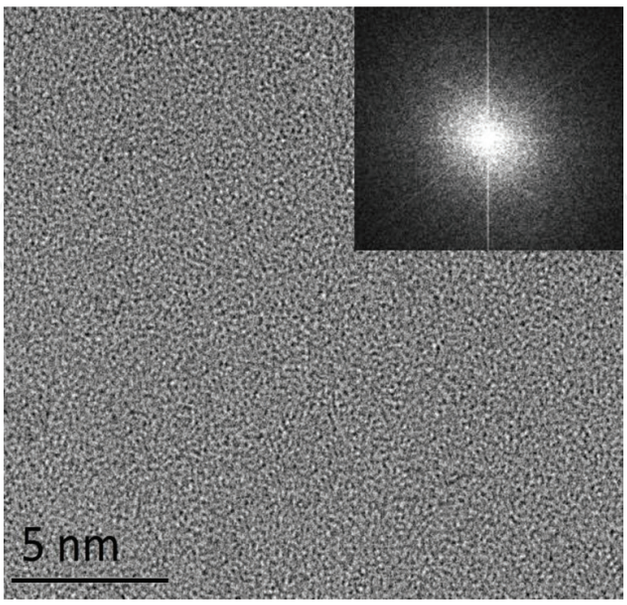

Figure 8. HRTEM image and the corresponding FFT-SAD of Al-35.4 at.%Fe showing a complete amorphous phase after 40 h of milling (reprinted with kind permission from reference [34], copyright 2015, Elsevier).

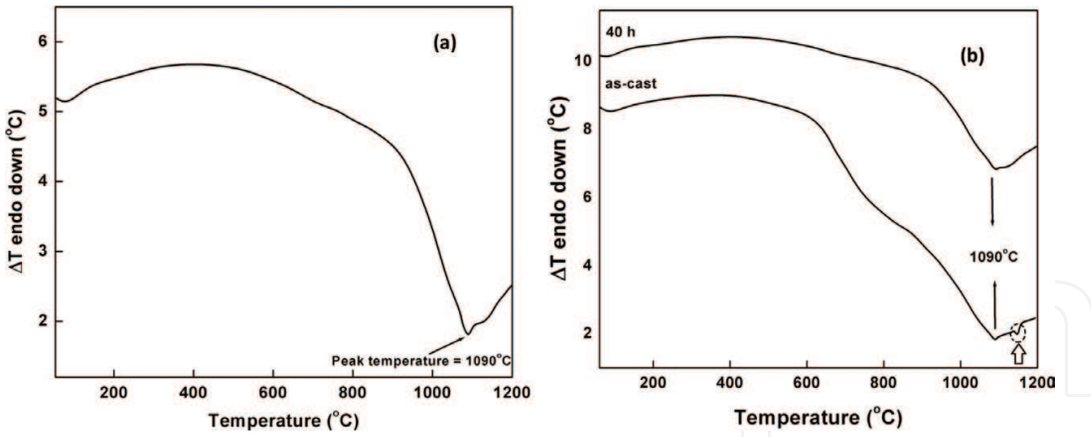

Figure 9. DTA traces of milled powders for (a) Al-25 at.%Fe and (b) Al-34.5 at.%Fe alloy (reprinted with kind permission from reference [34], copyright 2015, Elsevier).

Differential thermal analysis (DTA) trace of 50 h-milled Al-25 at.%Fe intermetallic powders is shown in **Figure 9a**. Upon heating the as-milled powders at a constant rate of 10°C/min, one exothermic peak at around 1090°C was revealed. An equilibrium diagram of Al-Fe [10] confirms that this peak corresponds to the melting point of the Al_5Fe_2 intermetallic phase, formed as a result of phase transformation of monoclinic Al_3Fe after high-energy ball milling. DTA curves of as-cast Al-34.5 at.%Fe alloy and ball-milled powder obtained after 40 h of milling are shown in **Figure 9b**. As marked by arrows, the thermal curves indicated the presence of two endothermic peaks for the as-cast alloy. According to the equilibrium phase diagram, the first peak at 1090°C corresponds to the melting point of Al_5Fe_2 intermetallic compound, and the second peak at a higher temperature (1149°C) as marked by an arrow is due to the melting of Al_2Fe. A single exothermic peak around 1090°C corresponding to Al_5Fe_2 phase formed as a result of transformation of an Al_2Fe intermetallic phase to a high-symmetry phase Al_5Fe_2 after high-energy milling was evidenced from DTA trace of 40 h milled powders. Thermal analysis results agree well with the XRD results as shown in **Figure 7**, where the pattern corresponds to both Al_5Fe_2 and Al_2Fe phases for as-cast alloy and a single Al_5Fe_2 phase for 40 h milled powders. The calculation of free energy of equilibrium phases was carried out based on the improved Miedema's model (Zhang model). **Table 3** gives the data of Al and Fe necessary for the calculation of Gibbs free energy. The variation of ΔG (for amorphous, two intermetallic compounds and crystalline solid solutions) as a function of composition for different values of d_c is shown in **Figure 10**. It is observed that the free energy of crystalline phase of a large crystallite size is lower compared to that of amorphous phase. Henceforth, for the entire compositional range, the crystalline phase is expected to be more stable than the amorphous phase. As the Gibbs free energy is minimum at the corresponding composition, the intermetallic thus found is considered as a most stable phase. The two intermetallic phases (Al_3Fe and Al_2Fe) corresponding to the compositions Al-25 at.% Fe and Al-34.5 at.% Fe are the most stable phases compared to the solid solution phase. Al_3Fe phase can transform to the amorphous phase at $d_c < 20$ nm, and to convert Al_2Fe phase into the amorphous state, the phase grain size should be below 30 nm. The results obtained from XRD and TEM analysis of the milled powder support that

Element	$n^{1/3}$ (cm^{-1})	Φ (V)	K (GPa)	μ (GPa)	T_m (K)	$V^{2/3}$ (cm^2)	γ (erg/cm^2)	ΔH_f (kJ/mole)
Al	1.39	4.2	75.83	26	933	4.6	340	10.83
Fe	1.77	4.93	164.78	82	1812	3.7	756	13.86

Table 3. Data of Al and Fe taken for thermodynamic calculation.

the phases are intermetallic prior to milling and amorphous after milling at the composition of Al-25 at.% Fe and Al-34.5 at.% Fe.

2.2. Mechanical properties

Figure 11a shows the milling time dependence of Vickers hardness for Al-25 at.%Fe alloy for various milled powders. The hardness increases with an increase in the milling time and reaches its maximum value between 20 and 30 h of milling and then decreased. A higher hardness value of about 8.6 GPa resulted at 30 h of milling. Thus, the optimum milling time for the studied composition is 30 h. The formation of intermetallic phase, η-Al_5Fe_2, and its co-existence with amorphous phase could be the reason for the observed peak in hardness values. However, for Al-20 at.%Fe alloy, the microhardness of 12.4 GPa was reported for 20 h of MA followed by cold consolidation and subsequent annealing at 673 K for 2 h [39]. **Figure 11b** shows the change in microhardness as a function of reciprocal square root of the grain size. It is evident that up to a grain size of about 42 nm, the values of hardness increase linearly with the reciprocal square root of the grain size. Over the range of grain sizes from 132 to 42 nm, the Hall-Petch (HP) behaviour is established. Further, the HP slope, which describes grain size

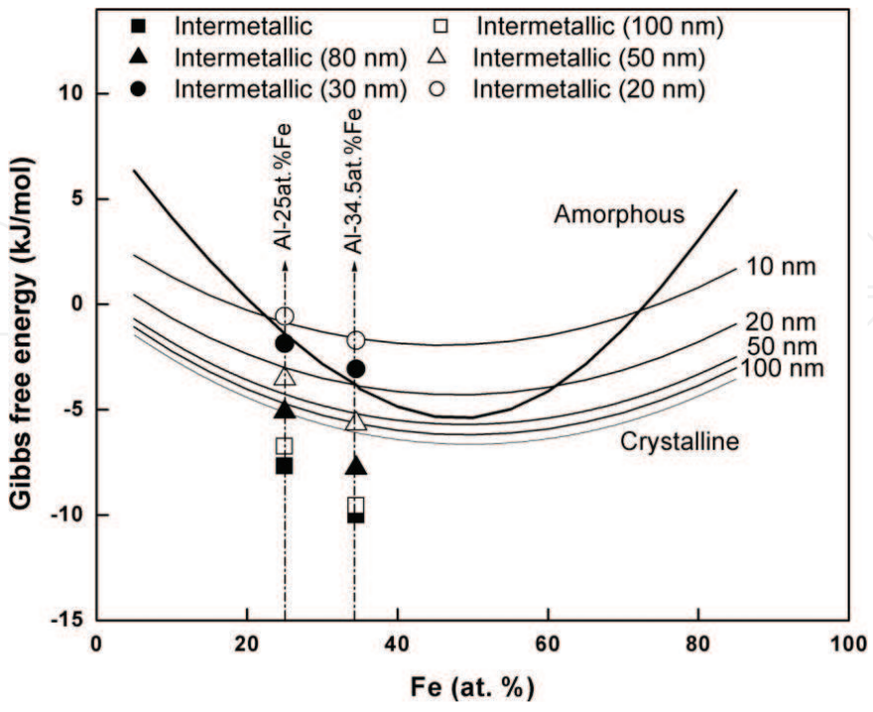

Figure 10. Gibbs free energy of the amorphous, solid solution and intermetallic phases of Al-Fe system as a function of composition and grain size.

http://dx.doi.org/10.5772/intechopen.73944

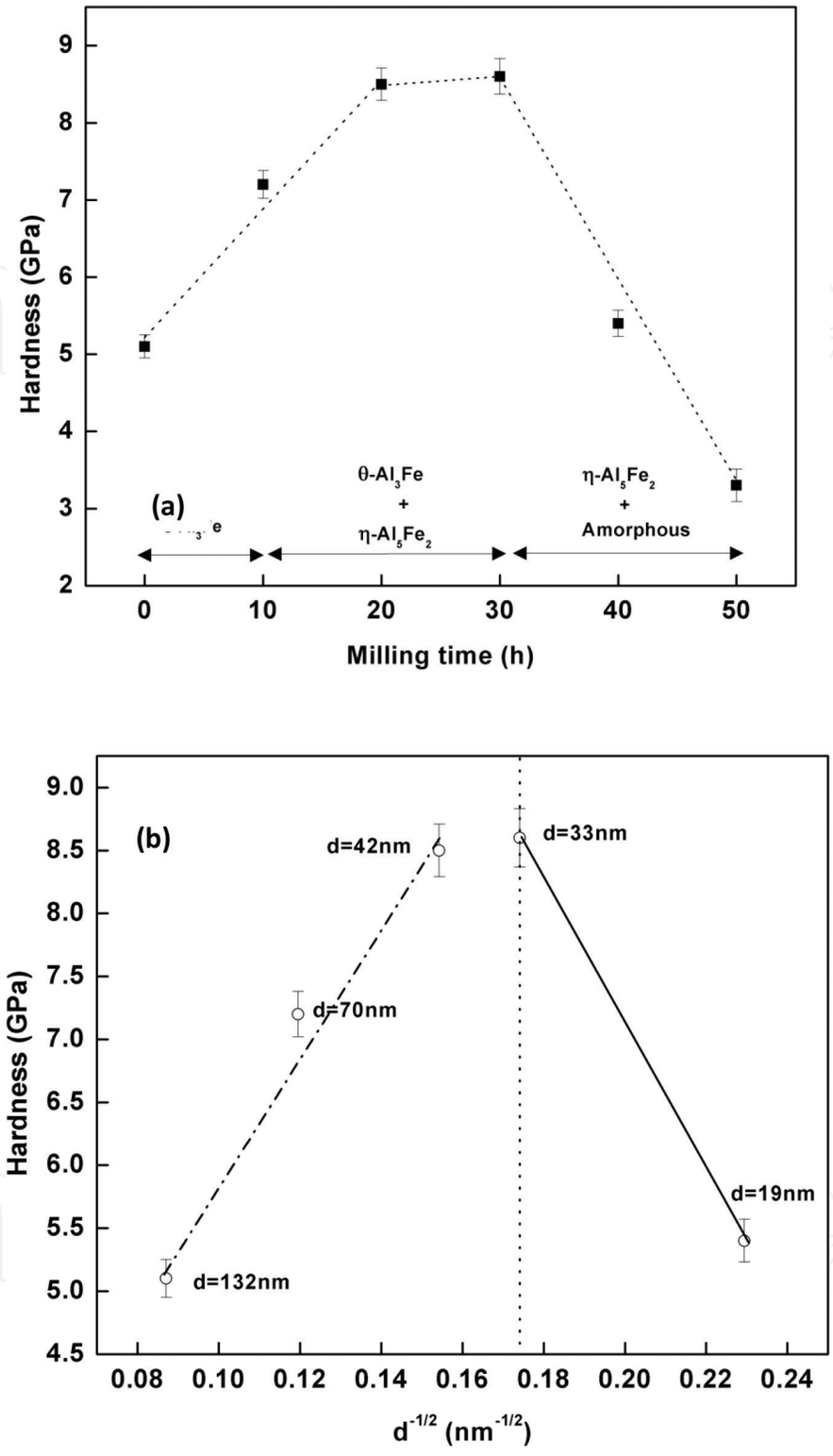

Figure 11. (a) Variation of microhardness as a function of milling time for Al-25 at.%Fe alloy showing the phase sequence and softening behaviour, (b) variation of microhardness as a function of square root of the grain size to test the Hall-Petch relationship for Al-25 at.%Fe alloy (reprinted with kind permission from reference [34], copyright 2015, Elsevier).

sensitivity, also have a similar value to that found for conventional grain sizes. This behaviour is ascribed to the refinement in the grain size produced as a result of MM. However, it is worth noting that when the crystallite sizes drop below 42 nm, the slope of the Hall-Petch plot

becomes negative. The evidenced effect could be due to a softening behaviour, an attribute described as an inverse H-P phenomenon [28, 29]. Theoretically, the critical value of the grain size below which the plot becomes negative can be calculated from Eq. (4)

$$\sigma = \sigma_0 + k\, d^{-\frac{1}{2}} \tag{4}$$

To examine the discrepancy involved in a dislocation pile-up mechanism related to a softening behaviour, the critical grain size was calculated and found that the theoretical value obtained was about 8 nm in comparison to the experimental value of 42 nm. It can be concluded that the presence of competing/contributing effects of nanocrystalline and amorphous phase could be the reason for the differences observed. Though the critical grain size for nanocrystalline materials where softening occurs can be predicted by a dislocation pile-up model, it fails for composite structure involving nanocrystalline and amorphous phase. **Figure 12** shows the microhardness variation with a milling time for Al-30 at.% Fe alloy. It is apparent from the plot that a single Al_5Fe_2 intermetallic phase subjected to MM resulted in Hall-Petch (HP) break-down and showed two distinct behaviours. The break-down of Hall-Petch for the averaged hardness can be attributed to the deformation mechanism and structure that occur due to mechanical milling. The HP slope decreases below a critical grain size and becomes negative, indicating an inverse Hall-Petch (IHP) behaviour. The HP strengthening has been ascribed to the pile-up of dislocations and their resistance to slip transfer. However, HP behaviour for grain size ranging from

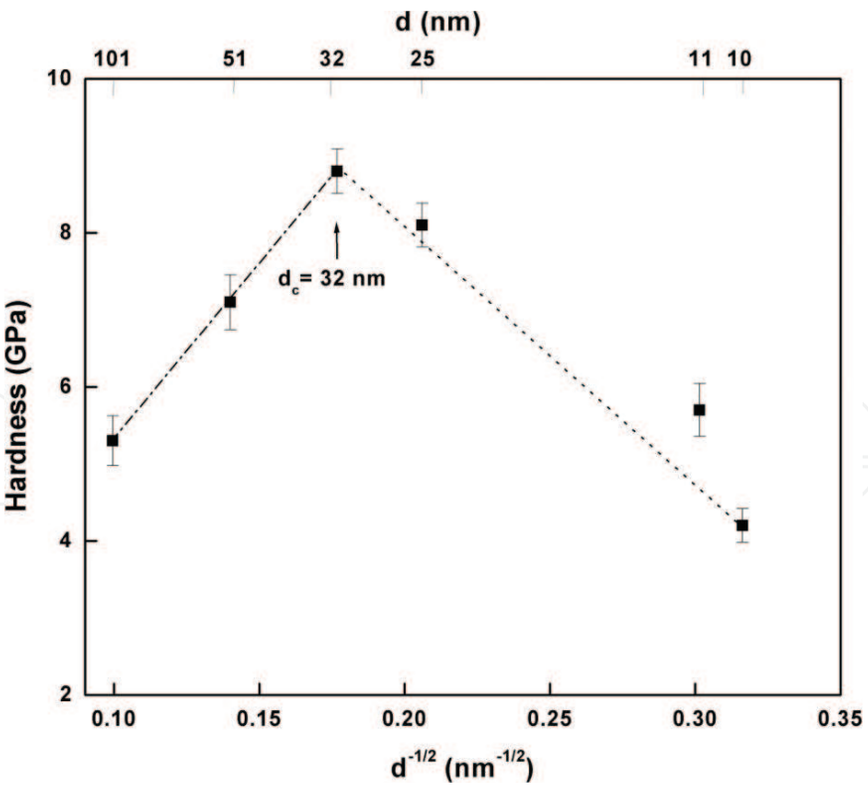

Figure 12. Hall-Petch plot of hardness of Al_5Fe_2 intermetallic against inverse square root of grain size showing transition from conventional Hall-Petch behaviour to inverse Hall-Petch behaviour (reprinted with kind permission from reference [35], copyright 2016, Taylor & Francis).

http://dx.doi.org/10.5772/intechopen.73944

101 to 32 nm and an IHP behaviour for grain sizes less than 32 nm was observed. The variation of microhardness as a function of milling time for Al-34.5 at.%Fe alloy is shown in **Figure 13**. The figure clearly demonstrates that the hardness of the alloy increased with increasing the milling time at the early stage and after prolonged milling reveals softening during the formation of amorphous phase. The hardness values increase with an increase in the milling time, which is an indicative of the formation of amorphous phase along with crystalline intermetallic phase. A softening behaviour observed at higher milling durations can be attributed to the high volume fraction of grain boundaries resulting in an increased triple junction leading to a grain boundary sliding [40]. The transition from hardening to softening behaviours that occurs in an amorphous phase could be ascribed to mechanisms such as a decrease in the interfacial excess volume and free volume model [29]. However, detailed investigation regarding this issue is needed to understand the softening behaviour. The typical load-displacement curves showing elastic-plastic material response for intermetallic phases milled for various durations, for indentations made to peak loads of 20 mN at room temperature, are presented in **Figure 14a** and **b**. Under the same conditions, the force displacement curves showed significant differences manifested not only by the shapes of the load-penetration depth but also by the maximum penetration depth attained. The microstructure of the intermetallic phases and its transformation during milling causes difference in the mechanical properties [29, 40] as evidenced in curves. The standard procedure according to Oliver and Pharr [33] (Oliver et al. (2004)) was employed to calculate the elastic modulus and hardness values. These parameters, estimated from the curve, are given in **Table 4**. The evolution of elastic modulus with a milling time indicates a relative complex effect of the phase formation/transformation in Al-Fe alloys.

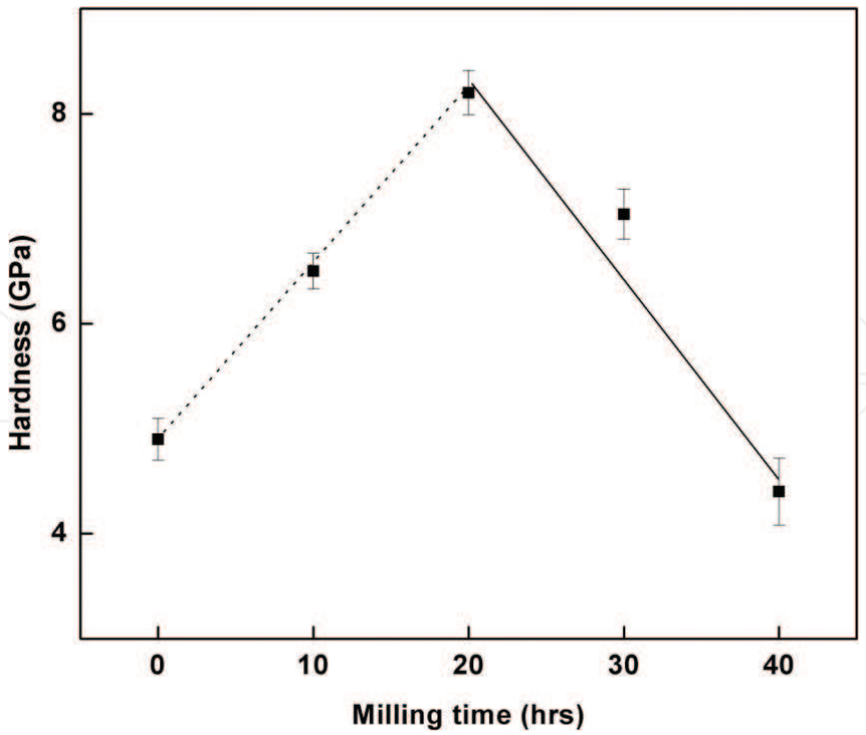

Figure 13. Microhardness variation as a function of milling time for Al-34.5 at.%Fe alloy showing transition from hardening to softening behaviour (reprinted with kind permission from reference [34], copyright 2015, Elsevier).

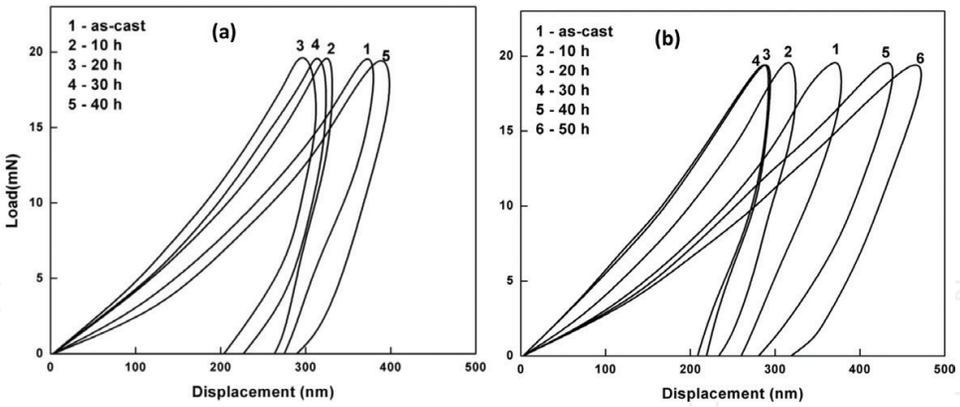

Figure 14. Nanoindentation load-displacement curves for (a) Al-25 at.%Fe and (b) Al-34.5 at.%Fe alloy at varying milling times (reprinted with kind permission from reference [34], copyright 2015, Elsevier).

Material	Hardness (GPa)						Elastic modulus (GPa)					
	Milling time (h)											
	0	10	20	30	40	50	0	10	20	30	40	50
Al-25 at.%Fe	7.2	7.8	9.3	8.2	6.5	5.0	121	139	168	146	116	89
Al-35.4 at.%Fe	6.1	7.0	8.8	7.6	4.9	—	100	129	157	138	88	—

Table 4. Hardness and elastic modulus of alloy powders of as-cast and for various durations of milling measured by nanoindentation (reprinted with kind permission from reference [34], copyright 2015, Elsevier).

The interatomic distance and the bonding strength between atoms, which is a representation of elastic modulus, are greatly influenced by the severe plastic deformation induced by mechanical milling. The increased hardness and elastic modulus resulted at the early stages of milling are due to the refinement in grain size which resists grain boundary motion. The maximum elastic modulus of 168 and 157 GPa and the peak hardness of about 9.3 and 8.8 GPa at 20 h were observed for Al-25 at.%Fe and Al-34.5 at.%Fe alloys, respectively. After a longer milling time where amorphous phase formation was evidenced, the hardness and elastic modulus values decreased to a factor of about two. The differences in the average values of 0.6 GPa between microhardness and nanohardness observed were ascribed to indentation size effect (ISE) [41].

3. Effect of grain size on mechanical properties

Mechanical property is an important consideration for the application of materials and depends fundamentally upon their microstructure on a variety of length scales and the nature of bonding among their constituent atoms. Mechanical deformation can be either elastic or plastic. Elastic deformation is effected through reversible changes in the interatomic spacing or the bending and stretching of bonds between atoms; it is governed by the elastic constants or moduli of a material. For metals, such deformation is in general relatively easy owing to the

non-local nature of metallic bonding, but for materials with a strong covalent or ionic bonding such as intermetallic compounds, it is difficult. Mechanical properties of nanocrystalline materials display an increasing interest. Reducing the grain sizes not only creates a big impact on the microstructures of the nanocrystalline materials but also alters their mechanical properties significantly. The most important mechanical properties of nanocrystalline metals and alloys include significantly increased hardness, strength and ductility, and so on with respect to the decreasing grain sizes [42]. The mechanical properties of NC materials not only depend on the average grain size but also depend on the grain size distribution and the microstructure, such as the grain boundary structures have a critical effect on their mechanical properties.

3.1. Inverse Hall-Petch effect in nanocrystalline materials

As suggested by the well-known Hall-Petch relationship, the mechanical properties of the material increase with the inverse square root of the grain size. However, as the grain size decreases to the submicrometre range, the *k* value (material-dependent constant) often referred to as the HP slope tends to decrease and when the grain size is decreased to less than 100 nm; the *k* value often becomes negative. The relationship between the strength of the nanostructured material and the grain size is very complicated. Since dislocation activity is almost absent in these materials, below a critical grain size, the HP relation becomes invalid. Deviations from the Hall-Petch relation were first reported by Chokshi et al. [43] on nanocrystalline copper and palladium, and this softening behaviour for nanocrystalline materials is the so-called inverse Hall-Petch effect, that is, hardness and strength decrease with a decrease in the grain size. At the nanoscale grain size where the dislocation activity is believed to be absent [44], below a critical grain size, k, the HP slope becomes negative, implying that the materials get softened. The break-down in the Hall-Petch trend has been attributed to different deformation mechanisms that become dominant once the grain size is reduced down to below a critical value [45]. The major interest involving the studies of strength has been to see if the HP relation holds at the smallest grain sizes. In this section, we present the results of recently observed IHP in the intermetallic Al_5Fe_2, and various deformation models in the present context of grain size softening will be discussed.

3.2. Deformation mechanisms

The expansion of the understanding of deformation of conventional polycrystalline materials to materials with grain sizes on the scale of nanometre is, at present, an evolving process. The experimental finding on inverse Hall-Petch has prompted various researches to propose models pertaining to their mechanism of deformation. Of the proposed models, different deformation mechanisms for nanocrystalline Al_5Fe_2 intermetallic are discussed subsequently.

3.2.1. Dislocation pile-up model

It is pertinent to point out that dislocation activities [46] have been shown to exist in some nanocrystalline materials. Nevertheless, the dislocation activity can be considered virtually absent in nanostructured materials where the grain size is lower than the minimum required distance to be maintained between the two dislocations. Therefore, the HP relation is expected to witness

a transition below a critical grain size, d_c. TEM and molecular dynamics (MD) simulation have also demonstrated that the grain boundaries can act as a source and a sink for dislocations. In nanomaterials, Hall-Petch behaviour breaks down because the grain is too small for dislocations to pile-up. In a polycrystalline sample, each individual grain will no longer be able to support more than one dislocation [48]. Using the concept proposed by Nieh and Wadsworth, Farghalli and co-workers [47, 48] developed a relationship between the critical grain size and hardness for the critical grain size below which softening occurs. Assuming that the stress field of a dislocation is valid at the nanoscale, and on the suggestion that fine grain sizes affect dislocation self-energy, a mathematical analysis was proposed and it leads to Eq. (5):

$$\frac{b}{d_{min}} = -\frac{2\beta H_i}{3G} + \frac{2}{3}\beta\left(\frac{H}{G}\right) \tag{5}$$

where b is the Burgers vector, H the measured hardness, H_0 the hardness equivalent of the applied stress at the moment of load application, G the shear modulus and β is a constant ranging equals 0.6 [47]. By using the material parameters for Al_5Fe_2 (b = 0.422 nm [49], G = 55 GPa β = 0.6, H = 8.8 GPa and H_0 = 0.45GPa [50] in the above equation,d_{min} d_{min} is estimated as 3.3 nm. Similarly, the critical grain size, after Nieh and Wadsworth [48] model, was calculated based on the following equation: $d_{min} \leq \frac{3Gb}{\pi(1-\nu)H}$, and it was found to be 3.58 nm. The calculated critical grain size (32 nm) was nearly eight times more than the values predicted based on dislocation pile-up models. Therefore, it is clear that dislocation-mediated process is not operative in these nanocrystalline intermetallics.

3.2.2. Grain boundary shearing/sliding model

It is clearly evident that the models based on dislocation pile-up could not account for grain size softening. For such fine grains, the deformation based on dislocation mechanisms becomes less dominant, and the mode of deformation based on grain boundary phase (via grain boundary shearing) comes into picture [51]. This would lead to a decrease in hardness and strength, since strain hardening due to dislocation will be absent and the grain boundary will be softer [52]. The deformation in nanocrystalline materials below a critical grain size has been analysed as a thermally activated process, determining the parameters such as activation energy (ΔF) and activation volume (ΔV). Conrad and Narayan [29] considered the thermally activated deformation and proposed a rate-controlling equation, which is given as

$$\dot{\gamma} = \frac{6\,b^*\nu_D}{d}\sinh\left(\frac{\nu\tau_e}{kT}\right)\exp\left(-\frac{\Delta F}{kT}\right) \tag{6}$$

The parameters in Eq. (6) are the Debye frequency, ν_D(10^{13} s^{-1}); the grain boundary width taken to be 3b^*, where b^* the atomic diameter; the effective stress, τ_e equals τ-τ_c where τ is the applied stress and τ_c is the threshold stress; v, the activation volume taken to be b^{*3}; ΔF the Helmholtz free energy; k the Boltzmann constant; and T is the temperature on absolute scale. For analysis, the shear rate $\dot{\gamma}$ is taken to be 10^{-3} s^{-1}. By assuming threshold stress, τ_c to be zero, the effective stress, τ_e, then equals the applied stress, τ, where $\tau = H/3\sqrt{3}$. The values of activation volume can

http://dx.doi.org/10.5772/intechopen.73944

be obtained from the slope of the best fit straight line from plot of *H* versus *ln d*. Eq. (6) can be rewritten in terms of hardness, by assuming *sinh* stress function to be exponential in one form and $\tau_c = 0$ in the other form. In view of the above and by taking logarithm, Eq. (6) can be modified as

$$H = 3\sqrt{3}\left\{\frac{kT}{v}\left[\ln\left(\frac{\dot{\gamma}}{3b^* v_D}\right) + \frac{\Delta F}{kT}\right] + \left(\frac{kT}{v}\right)\ln d\right\} \tag{7}$$

$$H = 3\sqrt{3}\left\{\frac{kT}{v}\left[\left(\frac{\dot{\gamma}}{6b^* v_D}\right)\exp\frac{\Delta F}{kT}\right]\right\}d \tag{8}$$

The model was validated for IHP regime of the current experimental data, and the experimentally observed and calculated hardness values of this system are shown in **Figure 15**. The degree of fit, as described by coefficient of correlation, for all the three expressions H_v versus ln(L), H_v versus L (these two describe the rigorous and approximate forms of the relationship in the model by Conrad and Narayan [29]) and H_v versus $(L\text{-}L_0)^{0.5}/L$ [53], is very similar, and the findings are presented in **Table 5**. On this basis, both the models are acceptable. The preceding discussion shows that although the model proposed by Conard and Narayan explains the IHP effect, the parameters used for validation is quite unreasonable: (1) the effective stress is taken to be equal to the applied stress, that is, the strain-rate sensitivity index, m = 1.0. However, in nanocrystalline materials at room temperature, the value of m is in the range of 0.02–0.08 [54, 55] and (2) further, the strain rate was assumed as 10^{-3} s^{-1}, but according to [56, 57], the strain rate lies in the range of 5×10^{-2} to 5×10^{-4} s^{-1}. Thus, the experimental data were analysed using both the strain rate values and the free energy of activation, ΔF_0, for the rate-controlling process (mesoscopic GBS), and refined values of γ_0 were determined as a function of strain rate and the results are presented in **Table 6**. The following observations are interesting: the relative change in hardness as one goes from the HP to the IHP region is much less in intermetallics than in nanocrystalline materials. This aspect needs further study. However, it is clear that the observed IHP effect in intermetallics also could be explained in terms of the mesoscopic grain boundary sliding controlled flow process, as with the other classes of materials. Finally, as the value of N for the system (**Table 6**) is less than one, it follows from the model [58–60] that the plane interface formation in these intermetallics of the studied grain size ranges is the result of dislocations/partial dislocations being emitted from the deforming boundary, which then traverse the grain and get absorbed at the opposite boundary [58, 59]. The value of ΔF equals 70 kJ/mol and v equals $(1.887 \times 10^{-10})^3$ nm^3 was obtained by plotting experimental hardness against ln d. A plot of H versus $ln\ d$ for the IHP data is presented in **Figure 16**. In addition, ΔF values obtained by linear fit of both experimental hardness values against *ln d* and *d* resulted in a reasonable agreement. The activation energy for grain boundary diffusion of this type of intermetallics [29] was found to be slightly higher compared to the present activation energy obtained from this analysis. The results are somewhat in accordance with the previous work on nano-quasicrystalline materials, which proposed a similar approach for the observed softening related to inverse Hall-Petch behaviour [51]. Using this model, the predicted and

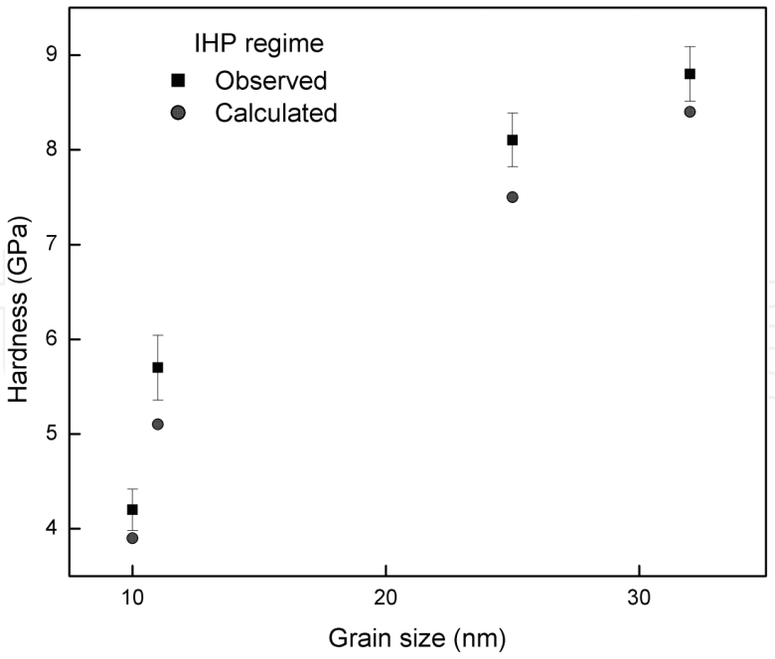

Figure 15. Hardness versus grain size in IHP regime observed values and calculated values obtained using Eq. (8) (reprinted with kind permission from reference [35], copyright 2016, Taylor & Francis).

System	L, nm	H, GPa	Correlation coefficient of H and		
			ln(L)	L	$(L-L)^{0.5}/L$
Al_5Fe_2	32.0	8.8	0.970	0.949	0.968
	23.6	8.1			
	11.0	5.7			
	10.0	4.2			

Table 5. Degree of fit for the three relations: $H \propto \ln(L)$, $H \propto L$ and $H \propto (L - L)\,0.5/L$ (reprinted with kind permission from reference [53], copyright 2016, Elsevier).

the current experimental data were plotted, and it was shown that qualitatively the fit is acceptable (**Figure 15**). The detailed examination showed that the correlation coefficient calculated based on grain boundary sliding using H_v versus $d^{0.5}$ plot and grain boundary shearing calculated based on H_v versus d and H_v versus $ln\ (d)$ resulted in identical values, proposing that both the models can describe the so-called inverse Hall-Petch effect. Despite the abovementioned similarity, manifest difference exists in the activation energy for the rate-controlling process due to their atomistic approach in the rate-controlling process. In case of grain boundary shearing approach, the effective stress is considered as the applied stress, that is, the strain-rate sensitivity index, m, equals 1.0. Nevertheless, in nanocrystalline materials, "m" ranges between 0.02 and 0.08 at room temperature. In general, it was pointed out that some of the approximations made in atomistic grain boundary shearing model to explain are questionable [34].

System	N	L, nm	τ_o, GPa	γ_0, refined*	ΔF_0, kJ/mol	
					$\dot{\gamma} = 5 \times 10^{-2}$, s^{-1}	$\dot{\gamma} = 5 \times 10^{-4}$, s^{-1}
Al_5Fe_2	0.8458	32.0	1.52	0.0711	157.73	170.37
		23.6	1.74			
		11.0	2.27			
		10.0	2.33			

G = 61.8 GPa.*As the strain rates in the indentation tests are assumed to be in the range of 5×10^{-2} s^{-1} to 5×10^{-4} s^{-1} [56], refined γ_0 values were obtained for the mean values of ΔF_0 for this range.

Table 6. The average shear strain in the basic unit of sliding, the number of grain boundaries that align to form a plane interface during mesoscopic boundary sliding and the free energy of activation for the rate-controlling GBS process (reprinted with kind permission from reference [53], copyright 2015, Elsevier).

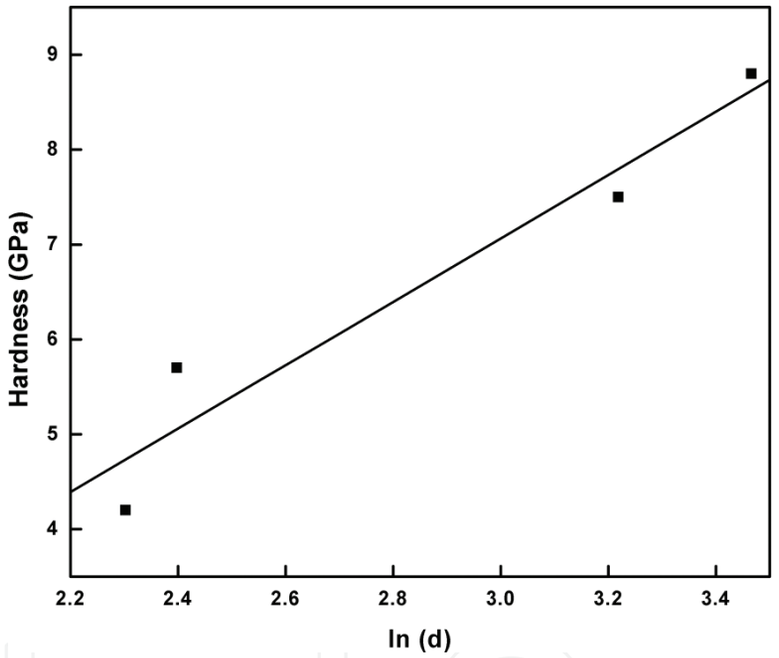

Figure 16. Plot of hardness *H*versus ln*d* for IHP regime (reprinted with kind permission from reference [35], copyright 2016, Taylor & Francis).

4. Conclusion

In this section, the recent progress in the synthesis of Al-Fe intermetallics and their softening behaviour using various deformation mechanisms is discussed. In this process, Al-25 at.%Fe and Al-34.5 at.%Fe alloys resulted in Al_3Fe and Al_2Fe intermetallic phases after normal casting and annealing routes. Monoclinic Al_3Fe and triclinic Al_2Fe phase was found to be unstable under high-energy milling condition and transformed to orthorhombic Al_5Fe_2 phase. Nanocrystalline and amorphous phase co-exist for 30 h of milling where the maximum hardness was observed. A microhardness of Al-25 at.%Fe alloy showed strengthening down to a

grain size of 42 nm, and Hall-Petch behaviour was thus established over the range of grain sizes from 132 to 42 nm. At the smallest grain size (33 nm), the slope of HP plot becomes negative indicating IHP behaviour.

In addition, Al_5Fe_2 resulted from Al-30%Fe alloy resulting in the formation of nanocrystalline intermetallic and was found to be quite stable under the present experimental conditions, and the crystallite size of it decreases up to 10 nm with an increase in the milling time. Microhardness measurements of single Al_5Fe_2 nanocrystalline intermetallic phase produced by mechanical milling resulted in Hall-Petch (HP) break-down and showed two distinct behaviours. The break-down of HP for the averaged microhardness measurements was found to be due to the transition of deformation mechanism from dislocation activity to grain boundary sliding. Dislocation models could not intend the critical grain size at which the HP relation breaks down, and so models based on grain boundaries were considered. Detailed analysis showed that models based on grain boundaries namely grain boundary sliding and thermally activated grain boundary shearing seem to be reasonable in explaining the IHP effect. Grain boundary sliding is ascribed to be a viable deformation mechanism resulting in a softening behaviour observed in this system.

Acknowledgements

The authors are thankful to Dr. V.C. Srivastava and Prof. K.A. Padmanabhan for many stimulating discussions. One of the authors (Raviathul Basariya) gratefully acknowledges the financial support by L.S. Ameer Dheen, Chennai, India, in the form of Research Fellowship. Sections 2 and 3 of this chapter are reproduced with permission from References [34, 35] (©2015, 2016 Elsevier).

Author details

Mohammed Ishaq Raviathul Basariya[1]* and Nilay Krishna Mukhopadhyay[2]

*Address all correspondence to: ravia80@gmail.com

1 College of Engineering, Guindy Campus, Anna University, Chennai, Tamil Nadu, India

2 Department of Metallurgical Engineering, Indian Institute of Technology, Banaras Hindu University, Varanasi, Uttar Pradesh, India

References

[1] Darolia R. NiAl alloys for high temperature structure applications. The Journal of The Minerals, Metals & Materials Society. 1991;**43**(3):44

[2] Bohn R, Hanbold T, Birringer R, Gleiter H. Nanocrystalline intermetallic compounds-an approach to ductility? Scripta Metallurgica et Materialia. 1991;**25**:81

[3] Jang JS, Koch CC. The Hall-Petch relationship in nanocrystalline iron produced by ball milling. Scripta Metallurgica et Materialia. 1990;**24**:1599

[4] Koch CC, Cho YS. Nanocrystals by high energy ball milling. Nanostructured Materials. 1992;**1**:207

[5] Ermakov A, Yurchikov E, Barinov V. The magnetic properties of amorphous Y-Co alloy powders obtained by mechanical comminution. Physics of Metals and Metallography. 1981;**52**:50

[6] Yermakov AY, Yurchikov YY, Barinov VA. Magnetic properties of amorphous powders prepared by the mechanical grinding of Y-Co alloys. Fizika Metallov I Metallovedenie. 1981;**52**:1184

[7] Koch CC, Whittenberger JD. Review: Mechanical milling/alloying of intermetallics. Intermetallics. 1996;**4**:339

[8] Zou Y, Saji S, Kusabiraki T. Fast amorphization and crystallization in Al-Fe binary system by high-energy ball milling. Materials Research Bulletin. 2002; 37:123

[9] Ashby MF. Materials Selection in Mechanical Design. Butterworth-Heinemann: Burlington, MA; 2005

[10] Massalski TB. Binary Phase Diagram. OH, USA: American Society for Metals, Metals Park; 1986: 1 & 2

[11] Mukhopadhyay DK, Suryanarayana C, Froes FH. Structural evolution in mechanically alloyed Al-Fe powders. Metallurgical and Materials Transactions. 1995;**26**A:1939

[12] Krasnowski M, Kulik T. Nanocrystalline Al–Fe intermetallics—Lightweight alloys with high hardness. Intermetallics. 2010;**18**:47

[13] Mhadhbi M, Khitouni M, Escoda L, Sunol JJ, Dammak M. Microstructure evolution and mechanical properties of nanocrystalline FeAl obtained by mechanical alloying and cold consolidation. Journal of Alloys and Compounds. 2011;**509**:3293

[14] Krasnowski M, Kulik T. Nanocrystalline and amorphous Al–Fe alloys containing 60-85% of Al synthesised by mechanical alloying and phase transformations induced by heating of milling products. Materials Chemistry and Physics. 2009;**116**:631

[15] Corby RN, Black PJ. The structure of $FeAl_2$ by anomalous dispersion methods. Acta Crystallographica B. 1973;**29**:2669

[16] Mihalkovic M, Wisdom M. Structure and stability of Al_2Fe and Al_5Fe_2: First principles total energy and phonon calculations. Physical Review B. 2012;**85**:014113

[17] Zhou F, Luck R, Scheffer M, Lang D, Lu K. The crystallization process of amorphous Al80Fe20 alloy powders prepared by ball milling. Journal of Non-Crystalline Solids. 1999;**250**-25:704

[18] Huang B, Ishihara KN, Shingu PH. Metastable phases of Al–Fe system by mechanical alloying. Materials Science and Engineering: A. 1997;**231**:72

[19] Enzo S, Mulas G, Frattini R. The structure of mechanically alloyed AlxFe(1-x) end-products after annealing. Materials Science Forum. 1998;**269**-272:385

[20] Cardellini F, Contini V, Gupta R, Mazzone G, Montone A, Perin A, Principi G. Microstructural evolution of Al–Fe powder mixtures during high energy ball milling. Journal of Materials Science. 1998;**33**:2519

[21] Gasior W, Debski A, Moser Z. Formation enthalpy of intermetallic phases from Al-Fe system measured with solution calorimetric method. Intermetallics. 2012;**24**:99

[22] Romero-Romero JR, Luis Lopez-Miranda J, Esparza R, Espinosa-Medina MA, Rosas G. High-energy ball-milling of $FeAl_2$ and Fe_2Al_5 intermetallic systems. Materials Science Forum. 2013;**755**:47

[23] Zhang RF, Liu BX. Proposed model for calculating the standard formation enthalpy of binary transition-metal systems. Applied Physics Letters. 2002;**81**:1219

[24] Thompson JR, Politis C. Formation of amorphous Ti-Pd Alloys by mechanical alloying methods. Europhysics Letters. 1987;**3**:199

[25] Hellstern E, Fecht HJ, Garland C, Johnson WL. Multicomponent ultrafine microstructure. Materials Research Society. 1989;**132**:137

[26] Li S, Wang K, Sun L, Wang Z. A simple model for the refinement of nanocrystalline grain size during ball milling. Scripta Metallurgica et Materialia. 1992;**27**:437

[27] Eckert J, Holzer JC, Kill CE III, Johnson WL. Structural and thermodynamic properties of nanocrystalline fcc metals prepared by mechanical attrition. Journal of Materials Research. 1992;**7**:1751

[28] Padmanabhan KA, Dinda GP, Hahn H, Gleiter H. Inverse Hall-Petch and grain boundary sliding controlled flow in nanocrystalline materials. Materials science and Engineering: A. 2007;**452**-453:462

[29] Conrad H, Narayan J. On the grain size softening in nanocrystalline materials. Scripta Materialia. 2000;**42**:1025

[30] Zhu J, Miao Y, Guo JT. The effect of boron on charge density distribution in Ni_3Al. Acta Materialia. 1997;**45**:1989

[31] Xu S, Prasitthipayaong A, Pickel AD, Habib AH, McHenry ME. Mechanical properties of FeCo magnetic particles–based Sn-Ag-Cu solder composites. Applied Physics Letters. 2013;**102**:251909

[32] Chromik RR, Vinci RP, Allen SL, Notis MR. Nanoindentation measurements on Cu-Sn and Ag-Sn intermetallic formed in Pb-free solder joints. Journal of Materials Research. 2003;**18**:2251

[33] Oliver WC, Pharr GM. Measurement of hardness and elastic modulus by instrumented indentation: Advances in understanding and refinements to methodology. Journal of Materials Research. 2004;**19**:3

[34] Raviathul Basariya M, Roy RK, Pramanick AK, Srivastava VC, Mukhopadhyay NK. Structural transition and softening in Al-Fe intermetallic compounds induced by high energy ball milling. Materials Science and Engineering: A. 2015;**638**:282

[35] Raviathul Basariya M, Srivastava VC, Mukhopadhyay NK. Inverse Hall-Petch like behaviour in a mechanically milled nanocrystalline Al_5Fe_2 intermetallic phase. Philosophical Magazine. 2016;**96**:2445

[36] Burkhardt U, Yu G, Ellner M, Peters K. Structure refinement of the iron-aluminium phase with the approximate composition Fe_2Al_5. Acta Crystallographica. 1994;B50:313

[37] Gu N, Henley CL, Mihalkovic M. Co-rich decagonal Al-co-Ni: Predicting structure, orientation order and puckering. Philosophical Magazine. 2006;**86**:593

[38] Schwarz RB, Petrich RR, Saw CK. The synthesis of amorphous Ni-Ti alloy powders by mechanical alloying. Journal of Non-Crystalline Solids. 1985;**76**:281

[39] Nayak SS, Wollgarten M, Banhart J, Pabi SK, Murty BS. Nanocomposites and an extremely hard nanocrystalline intermetallic of Al-Fe alloys prepared by mechanical alloying. Materials Science Engineering: A. 2010;**527**:2370

[40] Carlton CE, Ferreira PJ. What is behind the inverse hall-Petch effect in nanocrystalline materials? Acta Materialia. 2007;**55**:3749

[41] Mukhopadhyay NK, Paufler P. Micro- and nanoindentation techniques for mechanical characterization of materials. International Materials Reviews. 2006;**51**:209

[42] Siegel RW, Fougere GE. Mechanical properties of nanophase metals. Nanostructured Materials. 1995;**6**:205

[43] Chokshi AH, Rosen A, Karch J, Gleiter H. On the validity of the Hall-petch relationship in nanocrystalline materials. Scripta Metallurgica. 1989;**23**:1679

[44] Koch CC, Narayan J. The inverse Hall-Petch effect—fact or artifact. Materials Research Society Symposia Proceedings. 2001;**634**:B5.1.1

[45] Koch CC. Optimization of strength and ductility in nanocrystalline and ultrafine grained metals. Scripta Materialia. 2003;**49**:657

[46] Froseth AG, Derlet PM, Van Swygenhoven H. Dislocations emitted from nanocrystalline grain boundaries: Nucleation and splitting distance. Acta Materialia. 2004;**52**:5863

[47] Mohamed FA, Yuwei Xun. Correlations between the minimum grain size produced by milling and material parameters. Materials Science and Engineering R: Reports. 2003;**354**:133

[48] Nieh TG, Wadsworth. Hall Petch relation in nanocrystalline solids. Scripta Metallurgica et Materialia. 1991;**25**:955

[49] Hirose S, Itoh T, Makita M, Fujii S, Arai S, Sasaki K, Saka H. Defect structure of deformed Fe_2Al_5 intermetallic compound. Intermetallics. 2003;**11**:633

[50] Weertman JR, Averback RS. Mechanical properties. In: Edelstein AS, Cammarata RC, editors. Nanocrystalline Materials: Synthesis, Properties and Applications. Bristol: Institute of Metals Publishing; 1996: 13

[51] Padmanabhan KA, Sripathi S, Hahn H, Gleiter H. Inverse Hall–Petch effect in quasi-and nanocrystalline materials. Materials Letters. 2014;**133**:151

[52] Jiang B, Weng GJ. A composite model for the grain-size dependence of yield stress of nanograined materials. Metallurgical and Materials Transactions A: Physical Metallurgy and Materials Science. 2003;**34**:765

[53] Raviathul Basariya M, Mukhopadhyay NK, Sripathi S, Padmanabhan KA. Grain size softening effect in intermetallics. Journal of Alloys and Compounds. 2016;**673**:199

[54] Padmanabhan KA. Mechanical properties of nanostructured materials. Materials Science and Engineering A. 2001;**304**:200

[55] Varam S, Rajulapati KV, BhanuSankaraRao K. Strain rate sensitivity studies on bulk nanocrystalline aluminium by nanoindentation. Journal of Alloys and Compounds. 2014;**585**:795

[56] Maier V, Durst K, Mueller J, Backes B, Hoppel HW, Goken M. Nanoindentation strain-rate jump tests for determining the local strain-rate sensitivity in nanocrystalline Ni and ultrafine-grained Al. Journal of Materials Research. 2011;**26**:1421

[57] Padmanabhan KA, Schlipf J. Model for grain boundary sliding and its relevance to optimal structural superplasticity: Part 1 e theory. Materials Science and Technology. 1996;**12**:391

[58] Padmanabhan KA, Gleiter H. Optimal structural superplasticity in metals and ceramics of microcrystalline- and nanocrystalline-grain sizes. Materials Science and Engineering A. 2004;**381**:28

[59] Venkatesh TA, Bhattacharya SS, Padmanabhan KA, Schlipf J. Model for grain boundary sliding and its relevance to optimal structural superplasticity. Materials Science and Technology. 1996;**12**:635

[60] Ali MNK, Scudino S, Samadi Khoshkhoo M, Stoica M, Srivastava VC, Uhlenwinkel V, Vaughan G, Suryanarayana C, Eckert J. Grain size softening effect in $Al_{62.5}Cu_{25}Fe_{12.5}$ nano-quasicrystals. Applied Physics Letters. 2013;**103**:201914